JOURNAL OF MATERIALS SCIENCE 5 (1970) 1027-1037

Directional Solidification of Eutectic and Off-Eutectic Au-Co Composites with and without Magnetic Field

P. R. SAHM, H. R. KILLIAS
Brown Boveri Research Center, 5401 Baden, Switzerland

A fibrous eutectic with Co fibres embedded in a Au-matrix can be obtained at $G/v \geq 2 \times 10^5$ deg/cm² where G = temperature gradient and v = growth velocity. Interfibre spacing $2R$ can be described by $R^2v = 1.2 \times 10^{-11}$ cm³/sec. Below $G/v = 2 \times 10^5$ deg/cm² cellular growth is observed. Fibre to blade transitions have been found over the entire range of growth velocities employed, i.e. between 10^{-5} and 10^{-2}cm/sec and are thought to be due to local growth perturbations. Composite growth under the influence of a magnetic field produces two effects: an orienting effect and a shape and size modification. Orienting occurs at slow growth rates, preferably, in hypereutectic alloys and is explained as a magnetic aligning of the ferromagnetic primary Co-precipitates. The shape and size modification which results in thick and segmented, caterpillar-like Co fibres, appears to be independent of growth rate (within the limits indicated above), occurs mainly in cell boundaries at all compositions, including hypoeutectic ones, and is thought to be due to a field induced enhancement of local temperature gradients.

1. Introduction

One of the primary interests of the modern user of composite materials is the choice of regular two-phase structures from a broad range of volume fractions. In growing such composites directly from eutectic and off-eutectic melts the experimental criterion normally consulted [1] is

$$G/v \geq m(C_e - C_n)/D \qquad (1)$$

signifying that a large temperature gradient G at the solid-liquid interface and a small growth rate v should favour crystallisation of regular composites with appreciable deviation of their nominal composition C_n from the eutectic composition C_e. D is the diffusion coefficient, m the slope of the liquidus line.

The previously reported effect [2] of a change in the composite solidification range through the use of a magnetic field appeared to warrant a more detailed investigation of the crystallisation behaviour of Au-Co alloys. This paper describes the results obtained in directional growth of eutectic and off-eutectic alloys with and without the application of a magnetic field.

2. Experimental Procedure

A vertical method of growth was utilised (fig. 1) in which evacuated fused silica tubes enclosed 3 mm diameter and 80 to 150 mm long samples. They were transported downward, i.e. with the solid-liquid interface moving up, through bifilarly wound Pt-Rh40 wire resistance heaters at speeds between 0.3 and 100 cm/h. The temperature gradient at the solidifying interface was varied by means of different heater arrangements, one of which is shown in the figure, and by the coolant into which the sample submerged after leaving the heater assembly. Air cooling gave temperature gradients between 10 and 50 deg/cm, increasing with the amount of superheating. Liquid metal (In—Ga eutectic) cooling gave gradients of more than 100 deg/cm. The temperature gradients were measured by 0.9 mm diameter Al_2O_3-tube enclosed Pt-Pt/Rh13 thermocouples that were inserted into a hole drilled into the sample. The entire heater assembly was contained in a concentric type magnet such that a continuously variable homogeneous magnetic field could be applied parallel to the direction of growth.

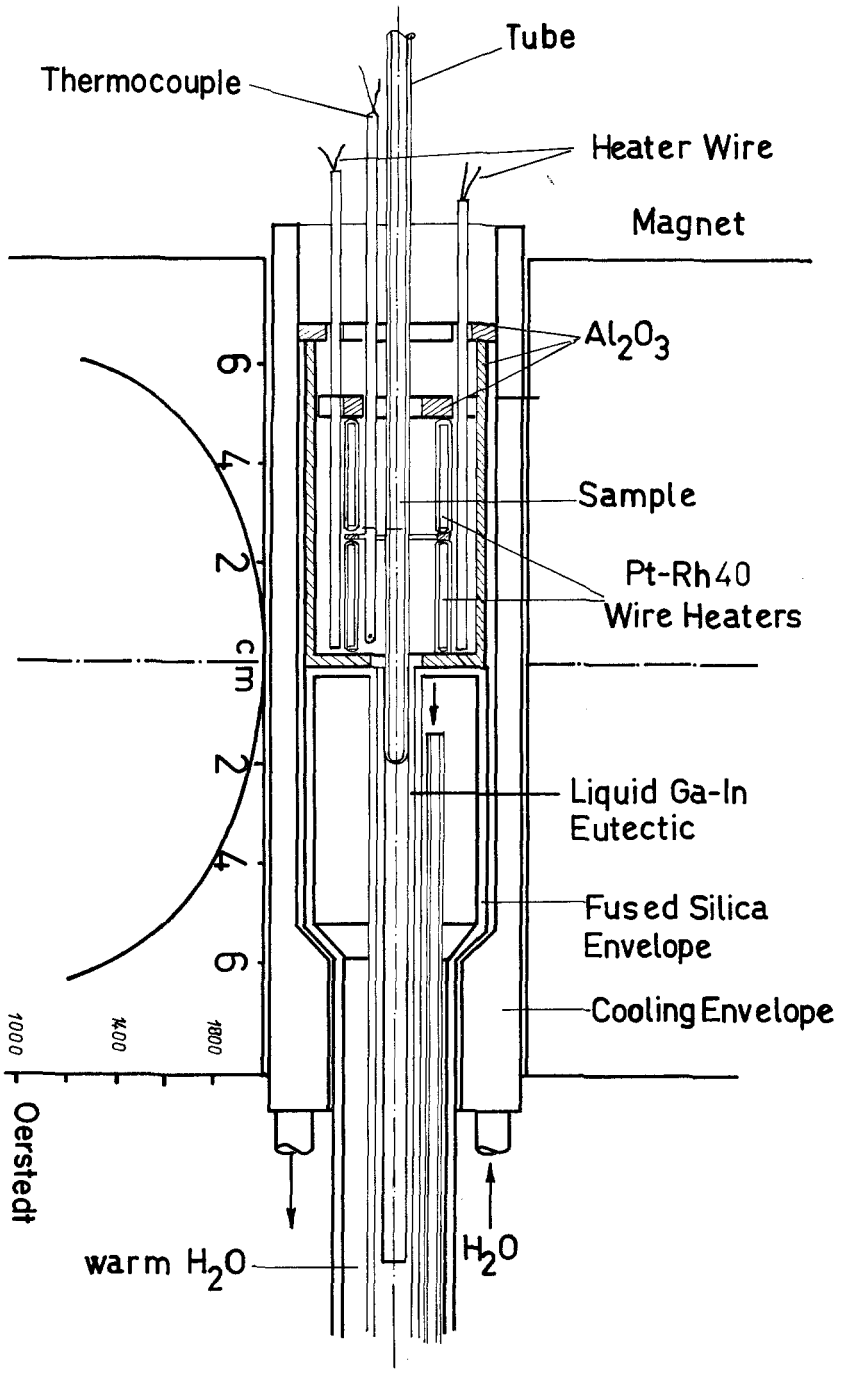

Figure 1 Apparatus for directional solidification in a magnetic field.

Prealloying of the samples was accomplished in H_2-atmosphere at temperatures around 1100° C utilising compact Au but powdered Co. The hydrogen treatment was necessary to remove the large oxygen content of the Co-powder. The prealloyed material was then inserted into fused silica tubes, evacuated at temperatures close to the eutectic temperature, and sealed off at vacua of 2×10^{-5} torr or better. The total metallic impurity level of the raw materials was of the

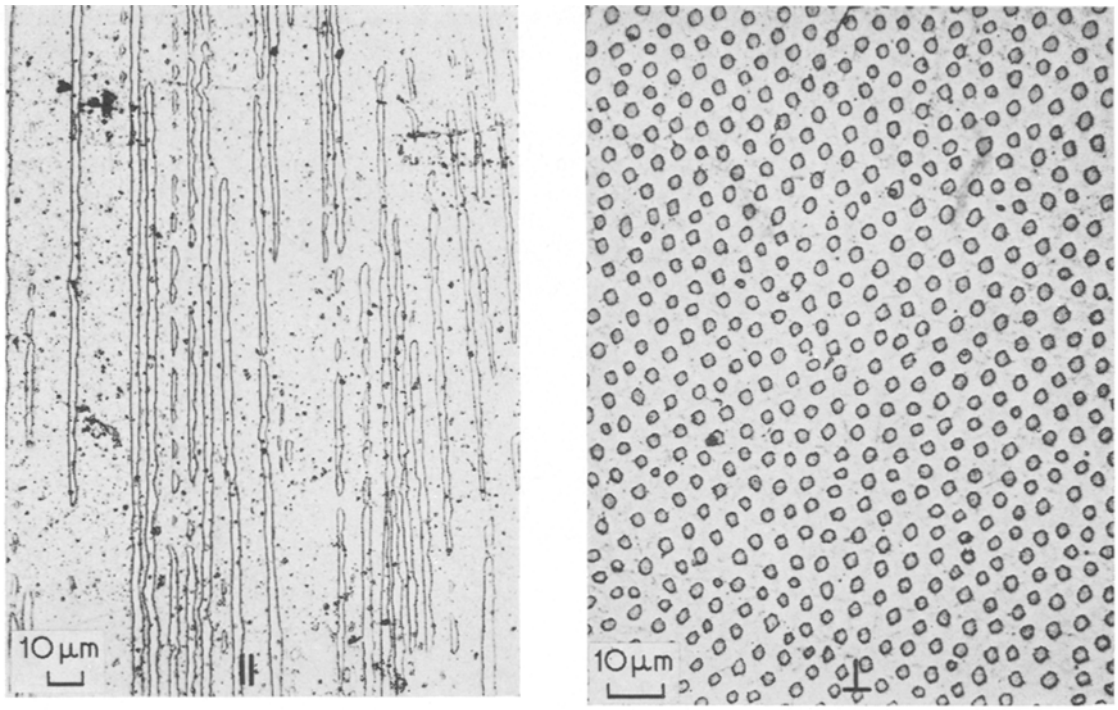

(a) (b)

Figure 2 Microstructure of fibrous Au-Co composite parallel (∥) and perpendicular (⊥) to growth direction.

order of 10 ppm by weight. For sample evaluation, light microscopy provided sections normal and parallel to the growth direction, the former of which were used to measure eutectic cell sizes and distances between Co-fibres. Powder X-ray analysis served as a method for determining the crystal structure of Co-fibres and Co-dendrites which were leached out of the matrix by a liquid mercury treatment at 100° C. Microprobe analysis yielded information on the Co-concentration retained in the Au-matrix and the Au-content in the Co-phase.

3. Results and Discussion

3.1. Growth Rate and Fibre Spacing

Under normal conditions, employing growth rates of $v = 5 \times 10^{-5}$ to 3×10^{-3} cm/sec, the Au-Co eutectic crystallised predominantly in fibrous form (fig. 2). The interfibre spacing $2R$ obtained in directional solidification can be satisfactorily described by the extremum condition type growth law congruent to the one quoted extensively in connection with lamellar eutectics [3] (fig. 3):

$$R^2 v = K_5 \qquad (2)$$

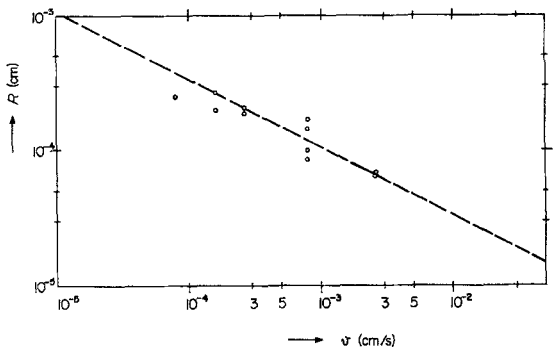

Figure 3 Relationship of characteristic distance between fibres $2R$ and growth rate v. Dashed line indicates slope 1/2 or R^2v = Konst. relationship.

where $K_5 = 1.2 \times 10^{-11}$ cm³/sec. This value is to be preferred to the one quoted in reference [2] since in the meantime additional, more accurate measurements have shifted the average value slightly from $K_5 = 1 \times 10^{-11}$ to 1.2×10^{-11}. Similar measurements by Livingston [4] resulted in $(2R)^2v = 6 \times 10^{-11}$, thus yielding $K_5 = 1.5 \times 10^{-11}$ which agrees well with our observation. Calculation of K_5 from corresponding states

estimates (see Appendix, equation A3) gives $K_5 = 2.9 \times 10^{-11}$ cm³/sec suggesting possibly, a smaller diffusion coefficient than that assumed in the calculation ($D = 10^{-5}$ cm²/sec).

Utilising the expression for K_5 derived by Jackson and Hunt [3], one can obtain an estimate of the average solid-liquid interface energy

$$\sigma_{\alpha,\beta-l} = (\sigma_{\alpha,l} + \sigma_{\beta,l})/2$$

assuming that $\sigma_{\beta,l}$ between Co-fibre and melt and $\sigma_{\alpha,l}$ between Au-matrix and melt may be equated. It yields:

$$\sigma_{\alpha,\beta-l} = 2K_5K'K_2(\zeta)\Delta c(1+\zeta)^{1/2}/DT_e \sin\bar{\alpha}_{\alpha,\beta}[\zeta(V_\alpha/L_\alpha m_\alpha) + (V_\beta/L_\beta m_\beta)] \quad (3)$$

(For explanation of terms and their values see Appendix.) Inserting numerical values into equation 3 gives $\sigma_{\alpha,\beta-l} = 79.3$ erg/cm². This value appears to be rather low when compared to the surface tensions of the pure metals against vacuum [5] of $\sigma_{Au} = 1200$ erg/cm² and $\sigma_{Co} = 1855$ erg/cm² even though lower values than these must be expected against the eutectic melt. Such a low σ-value, however, is not too surprising if one looks at the Au-Co equilibrium diagram [6] in fig. 4. It indicates that at $T_e = 996°$ C only 3.5 at. % Co segregation from the melt in the form of fibres increasing to about 25 at. %, i.e. about sevenfold, upon cooling to room temperature. Microprobe analysis yielded an amount of 2 at. % Co in the Au matrix corresponding closely to a calculated maximally possible 5 at. %. This means that the fibres crystallising out from the melt require an interface surface to volume ratio approximately three times higher than that appearing in the micrographs (e.g. fig. 2) thus requiring correspondingly lower interface energies $\sigma_{\alpha,\beta}$ and, since

$$\sigma_{\alpha,\beta} = \sigma_{\alpha,\beta-l} \cdot 2\cos\alpha_{\alpha,\beta},$$

also lower solid-liquid interface energies.

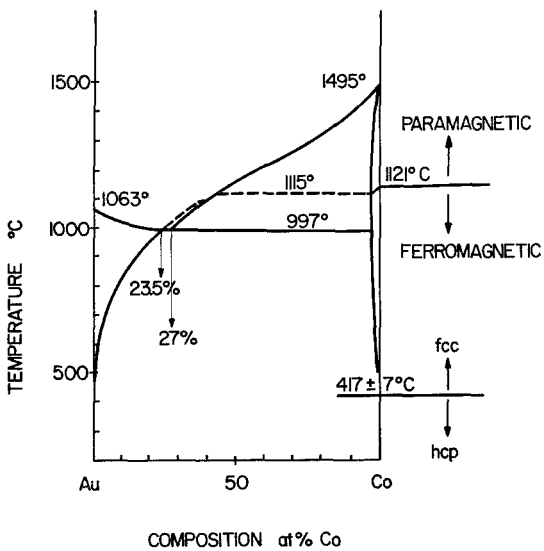

Figure 4 The binary Au-Co equilibrium diagram. The Curie temperature in the liquid phase is drawn according to Busch and Güntherodt, Solvay Congress 1969.

3.2. Range of Composite Growth

Fig. 5 illustrates the fit between the measured and the expected range of composite growth. The unusual logarithmic scale of G/v was chosen to

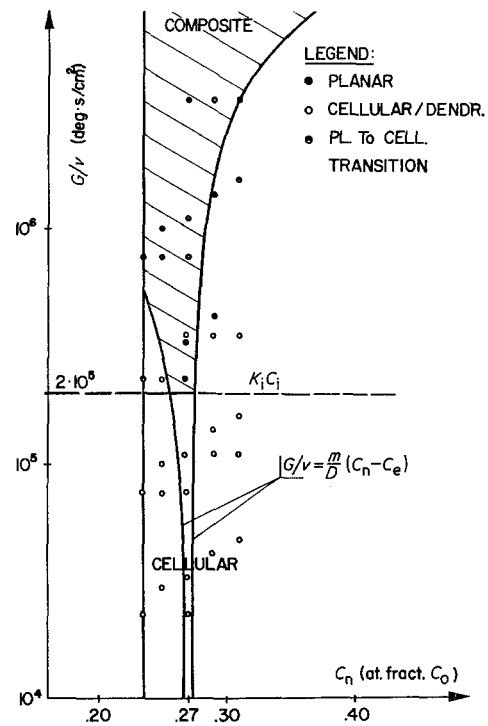

Figure 5 Range of composite growth in Au-Co alloys.

emphasise the limitations of the simple constitutional supercooling criterion of equation 1 in favour of Cline's modified version [7].

$$G/v = \frac{m}{D}(c_n - c_e) + K_1c_i \quad (4)$$

with $m = +160$ and -920 deg/at. fraction,

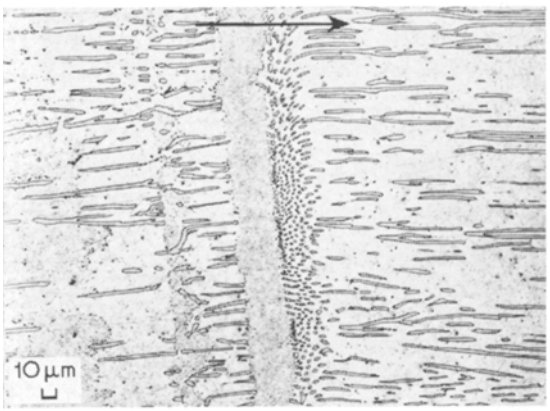

Figure 6 Growth band in hypoeutectic Au-Co alloy. Note numerous branching of fibres into growth direction.

$D = 10^{-5}$ cm²/sec, $c_e = 0.27$, and c_i standing for the concentration of an assumed impurity causing cellular growth to occur at $G/v < 2 \times 10^5$ deg sec/cm². On the Au-rich side of the eutectic no breakdown into a dendritic morphology was observed under steady state growth conditions, with the exceptions of loci where nucleation of the Co-phase was necessary to start off coupled growth, i.e. in the initial section of the ingot [8] or ahead of growth bands (fig. 6). The existence of growth bands also indicates the reality of a boundary layer ahead of the solid-liquid interface which in this particular case was Co-depleted with respect to the nominal composition of the alloy. Calculation of the equilibrium interface composition after Cline's analysis [7] suggests that the interface composition is slightly hypereutectic over the entire range of composite growth (fig. 5).

3.3. Cellular Growth

Since it is normally believed that cellular growth is caused by impurities, spectroscopic analysis was performed. It showed the presence of the order of 1 ppm by weight of Mg, Ag, Cu, Si, Fe, and Ca plus approximately 10 ppm of Pb. Although a segregation of these impurities to cell boundaries was not detectable by microprobe analysis, the measured total impurity concentration is obviously sufficient to account for the observed value of $K_i c_i$ of equation 4.

A closer examination of the cell boundaries (fig. 7) shows the presence of spherulitic Co-particles within the boundary zone. The formation of such particles implies a nucleation determined growth process in a strongly supercooled melt environment (as provided by a eutectic cell boundary) and requires a local negative temperature gradient around each growing spherulite [9]. The degree of supercooling is a function of the impurity level present and determines the slope in the experimentally found relationship for the eutectic cell diameter

$$D_c = 2.5 \times 10^{-2} (1/Gv)^{1/2} + 3.7 \times 10^{-3} \text{ cm}. \quad (5)$$

A relationship of this form has been observed by Rumball [10] in Al—Zn eutectics doped with Cu- and Ag-impurities.

It is interesting to note that micrographs such as fig. 7a suggest a helix-like growth of the eutectic cells. Similar observations have been made by Double *et al* [11] with respect to individual lamellas in lamellar eutectics.

3.4. Rod to Blade Transition

Local transitions from the fibrous into a blade-like morphology were observed in Au-Co eutectics as shown in fig. 8. Similar to findings reported in Al-Al_3Ni [12], Ag—Pb [13], GaSb—CrSb [14] and other eutectics, these transitions were preceded by an alignment of

TABLE I Compilation of magnetic field induced phenomena in the microstructure of Au-Co two-phase alloys.

Phenomenon	Orientation effect	Magnetic field	Compounding effect
Appearance of microstructure	normal, randomly oriented dendrites	$H = 0$	spherulitic particles: (*a*) in eutectic cell boundaries; (*b*) along growth bands
Appearance in microstructure	directionally aligned smoothened dendrite stalks	$H \neq 0$	caterpillar-like growth formations
Location in ingot	throughout entire volume	$H \neq 0$	(*a*) eutectic cell boundaries; (*b*) growth bands
Alloy composition	hypereutectic ($Cn \geq 27$ at. % Co)	$H \neq 0$	all ($c_n > 23.5$ at. % Co)
Growth rate	slow ($< 10^{-3}$ cm/sec)	$H \neq 0$	all (10^{-2} to 10^{-5} cm/sec)

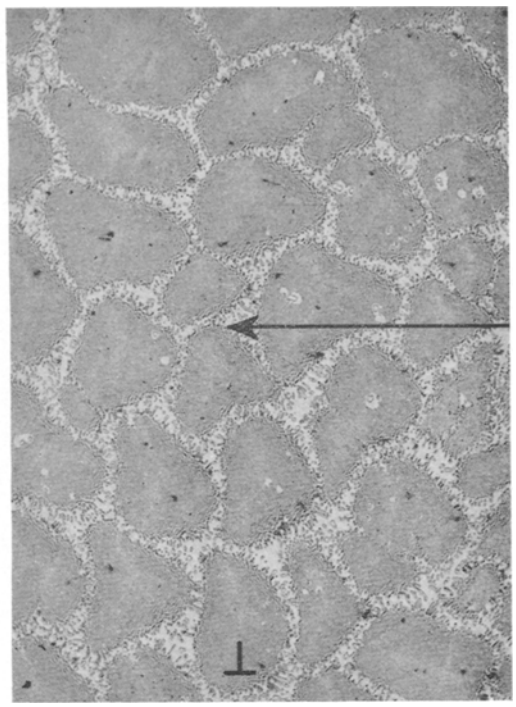

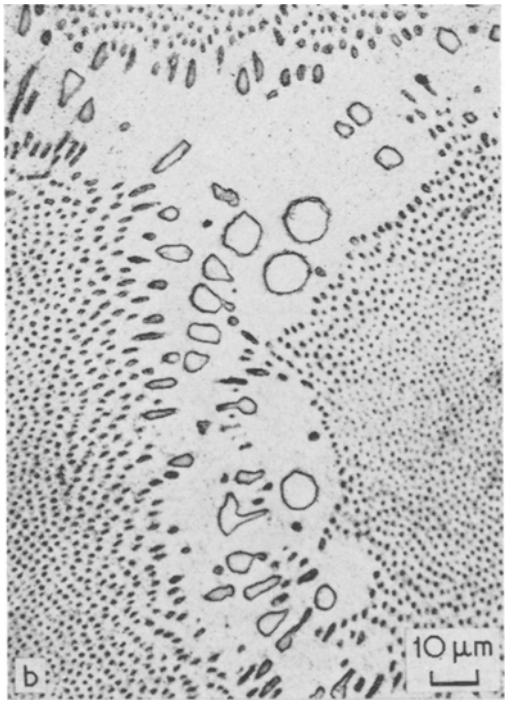

Figure 7 Cellular growth of eutectic Au-Co composite parallel (∥) and perpendicular (⊥) to growth direction (7a). (The arrow indicates the position of 7b.) Spherulite formation in colony boundaries (7b).

fibres into parallel lines in anticipation, as it were, of a later lamellar arrangement. While Livingston [4] reported a full-fledged transformation into blades at growth rates above approximately 10^{-1} cm/sec, the local transition phenomenon reported here prevailed at all growth rates and was particularly well distinguishable at the lowest rate of 8×10^{-5} cm/sec (fig. 8). The micrographs also show that the Co-rods were faceted, probably with smooth facets at the point of solidification, then assuming a rough appearance and irregular shape through solid state precipitation during cooling. The transition into the blade-like morphology appears to be simply due to the elongation of certain facets of the rods [15].

3.5. Solidification in a Magnetic Field

In the experiments referred to below a DC magnetic field of 2000 Oe was applied in parallel to the direction of growth as illustrated by fig. 1. The observed effects were (*a*) an orientation of the ferromagnetic component (orientation effect) and (*b*) a size and shape modification ("compounding effect"). Fig. 9 and table I summarise the effects. Orienting and compounding are discussed separately, even though a certain overlapping of the phenomena cannot be excluded.

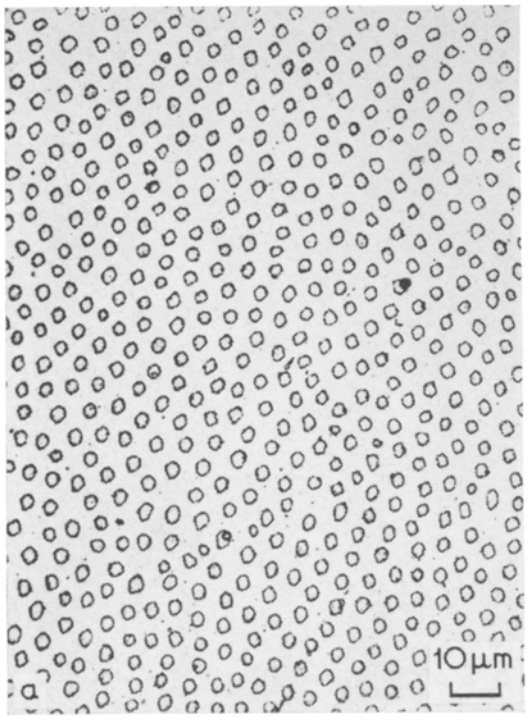

(a)

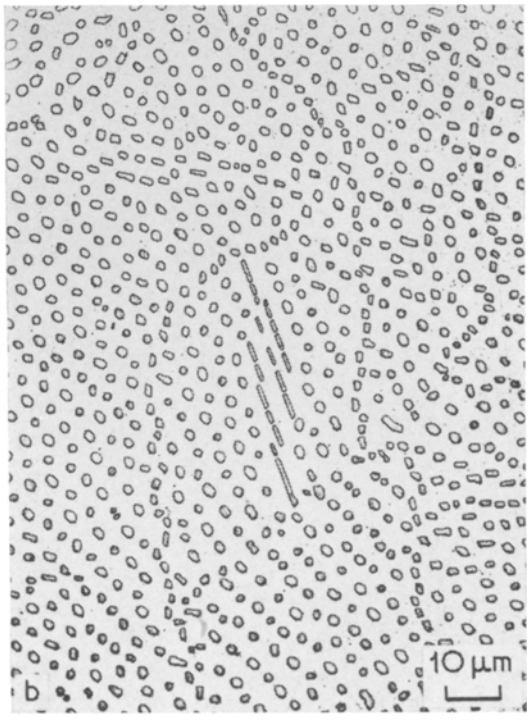

(b)

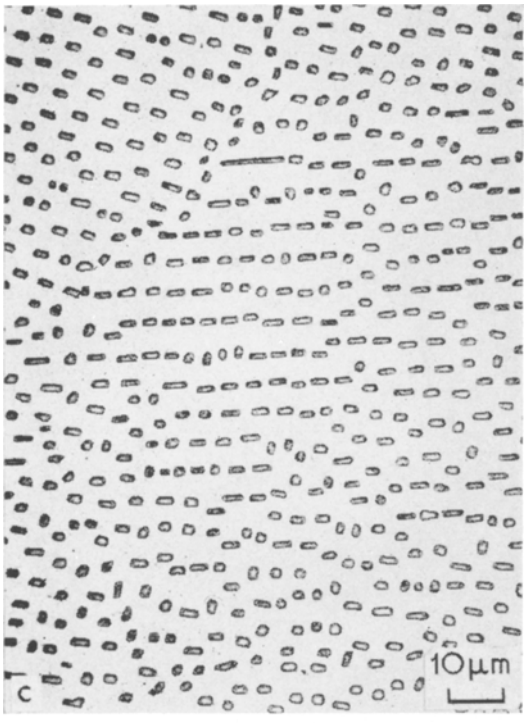

(c)

Figure 8 Fibre-to-blade transition in eutectic Au-Co composites. Sequence 9a-c shows a most ideal fibrous eutectic condition (a) progressing toward a ribbon—growth condition (c).

An orientation of ferromagnetic Co-dendrites in a metallic melt has been previously observed and explained in the Bi-Co system [16]. A similar explanation may be applied here: Primary Co-dendrites which are nucleated ahead of the advancing solid-liquid interface are aligned in parallel to the field. This results in an "enforced aligned growth condition" with two interfaces: the dendrite tip interface and the planar eutectic matrix interface (fig. 10). As in the case of Bi-Co alloys, the undercooling at the dendrite tip interface is small and not affected by the applied magnetic field.

The "enforced aligned growth condition" takes shape after an initial amassing (fig. 11) of numerous small dendrites or of dendrite debris (possibly stemming from larger broken dendrites). This amassing is thought to be caused by the field gradients which exist at the solid-liquid interface due to magnetisation differences between melt and solidified Au-Co alloy and, in

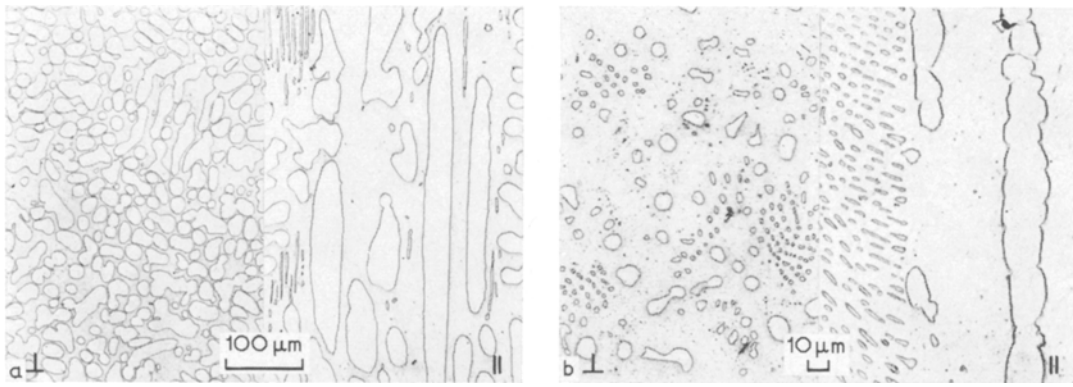

Figure 9 Magnetic field modified Co-precipitates in Au-Co alloys. Oriented Co-dendrites (9a) and segmented caterpillar-like Co fibres in eutectic cell boundaries (9b).

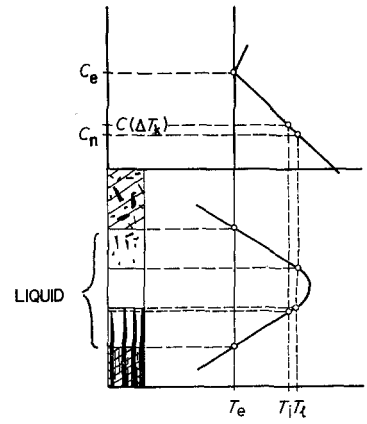

Figure 10 Illustration of the "enforced aligned growth condition". $T_l - T_i = \Delta T_k$ = kinetic undercooling.

addition, by the weak field gradient of approximately 40 Oe/cm which was superimposed on the liquid zone by the experimental set-up (fig. 1). A simple comparison between the force K_m exerted by this latter gradient in the direction opposite to the growth direction and the buoyancy force K_b and a 1 μm diameter Co-particle, of volume V and density δ_{Co} acting in the growth direction,

$$K_m = -H \frac{dH}{dz} V(\mu_{solid} - \mu_{liquid})$$
$$= 4 \times 10^{-8} \text{ dynes}$$

$$K_b = V(\delta_{Au} - \delta_{Co})\, g = 4.6 \times 10^{-11} \text{ dynes}$$

indicates that existing field gradients must have resulted in noticeable mechanical forces on the primary ferromagnetic Co-particles in the melt.

The smoothened appearance of Co-particles in both the dendrite debris sections (fig. 11a) and to a certain extent also in the "enforced aligned" section (fig. 11b) are ascribed to convection currents inducing re-solution of surface irregularities. Convection currents are caused, at least in part, by the rotation of Co-particles during alignment in the field.

In conclusion then, the orienting effect appears to be based on two phenomena:

(1) Field gradient forces overcompensate buoyancy forces acting on primary Co-precipitates

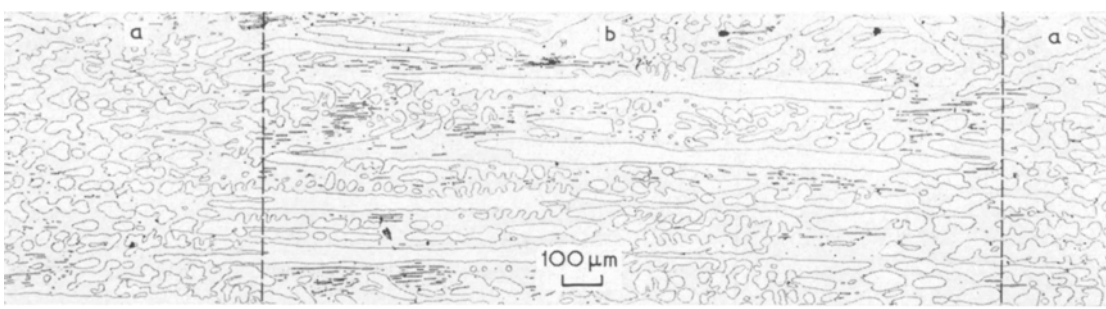

Figure 11 Typical sections found in magnetic field Co-dendrite stalk formation: fine particle section (a) and "enforced aligned growth" section (b).

and amass them at the solid-liquid interface and (2) the Co-precipitates become aligned parallel to the magnetic field lines with the longest dendrites yielding the smooth Co-dendrite stalks observed in the enforced aligned growth condition.

The *compounding effect* applies to the magnetic field induced formation of thick and segmented caterpillar-like Co-fibres where spherulites would normally be expected (table I). It appears to be more than a mechanical effect of aligning and conglomerating several spherical Co-particles into the formations shown in figs. 9b, 11, and 12, even though this possibility cannot entirely be excluded. It rather appears that these caterpillar-like formations are due to a direct influence of the field on the solidification mechanism. This assumption is supported by the microstructure in fig. 12 where the segmented thick fibres are seen to replace the normal eutectic structure in appreciable portions of the sample, having consumed, as it were, all those Co-atoms which normally would go into the regularly spaced Co-fibres of the eutectic.

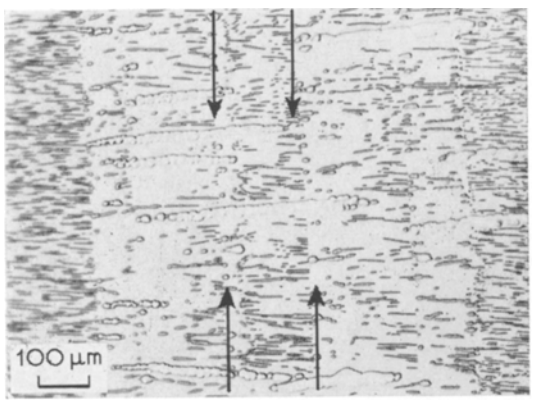

Figure 12 Growth band induced "compounding effect". Normal growth band coarsening of Co-phase would only yield spherulitic precipitates (see arrows in figure).

The segmented fibres originate at spherical Co-particles associated with growth bands (fig. 12) or with eutectic cell boundaries (fig. 7b). As pointed out previously, spherulitic growth presupposes a negative temperature gradient around each growing particle. It is now suggested that the magnetic field damps the perpendicular component of the microscopic convection current around the particle, thereby reduces the heat flow in this direction and thus enhances the temperature gradient at the top of the particle with respect to its sides [17, 18]. The particle, instead of continuing its spherical growth, will grow unidirectionally into the enhanced temperature gradient forming a second spherulite still attached to the first one. By repeating this process, a quasi-steady state growth condition may be achieved leading to the observed caterpillar-like thick Co-fibre formations aligned in the magnetic field direction.

It should be noted that for our interpretation of the compounding effect we have not made use of the fact that in liquid Au—Co alloys the existence of ferromagnetic interactions has been reported [19]. It is felt, however, that if the effect of ferromagnetism on such growth parameters as diffusion constant [20], surface energy, and undercooling would have to be taken into account, any such effect would be small when compared to the error limits of the order-of-magnitude calculations underlying the present interpretation.

4. Conclusions

Directional solidification of eutectic Au-Co alloys has yielded the following results.

(1) At $G/v \geq 2 \times 10^5$ deg.sec/cm^2 a regular fibrous composite is obtained with irregularly faceted Co-fibres embedded in a cobalt-saturated Au-matrix.

(2) The interfibre spacing $2R$ can be described by the relationship

$$R^2 v = 1.2 \times 10^{-11} \text{ cm}^3/\text{sec}.$$

(3) At $G/v \leq 2 \times 10^5$ deg.sec/cm^2 cellular growth is observed. The cell diameter can be described by

$$D_c = 2.5 \times 10^{-2} (1/Gv)^{1/2} + 3.7 \times 10^{-3} \text{ cm}.$$

(4) Local fibre-to-blade transitions have been observed over the entire range of growth velocities employed, ie between 10^{-5} and 10^{-2} cm/sec

(5) Composite growth under the influence of a magnetic field produces two effects: an orienting and a compounding effect.

(*a*) Orienting produces smooth Co-dendrite stalks and occurs at slow growth rates, preferably in hypereutectic alloys and is explained as a magnetic aligning of ferromagnetic primary Co-precipitates.

(*b*) Compounding produces segmented caterpillar like growth formations and appears to be independent of growth rate (between 10^{-2} and 10^{-5} cm/sec) and composition. It is associated with

eutectic cell boundaries and growth bands and is suggested to be due to field induced enhancement of local temperature gradients.

Acknowledgements

Thanks go to several people who were instrumentally involved in this work: Mrs B. Höhn for metallography, Mr F. Leher and Mr B. Kräutler for preparation of the alloys and their unidirectional growth, Mr Galetti and Drs Scheidegger and Hugi for X-ray and microprobe analyses. Special thanks are due to Mr A. Beck for many excellent suggestions in the course of this work.

Appendix

Jackson and Hunt's expression [3] for K_5 may be given as follows

$$K_5 = \frac{D.T_e.\sin\bar{\alpha}_{\alpha,\beta}}{\Delta c K_2(\zeta)(1+\zeta)^{1/2}} \left[\frac{\zeta\sigma_\alpha V_\alpha}{L_\alpha m_\alpha} + \frac{\sigma_\beta V_\beta}{L_\alpha m_\alpha}\right] \frac{1}{2K'} \quad \text{(A1)}$$

where:

D = diffusion coefficient in cm²/sec

T_e = eutectic temperature in °K

$\alpha_{\alpha,\beta}$ = groove angle between phases α and β at solid-liquid interface

$\bar{\alpha}_{\alpha,\beta}$ = 45° = assumed average groove angle

$\zeta = \frac{\phi_\beta}{\phi_\alpha} = \frac{\phi_\beta}{1-\phi_\beta}$ with $\phi_{\alpha,\beta}$ = volume fraction of phases α or β.

$\sigma_{\alpha,\beta-l}$ = solid (α or β)-liquid interface energy in erg/cm²

$V_{\alpha,\beta}$ = molar volume in cm³/mol

Δc = difference of solubility limits in at. fraction

$K_2(\zeta)$ = Bessel function dependent constant, see reference [3]

$L_{\alpha,\beta}$ = latent heat of fusion of phases α or β in cal/mol

$m_{\alpha,\beta}$ = liquidus slope in deg/at. fraction

K' = conversion factor: ergs into cal.

Assuming that

$$\sigma_\alpha = \sigma_\beta$$

one may arrive at an expression for the average solid-liquid interface energy:

$$\bar{\sigma}_{\alpha,\beta-l} = \frac{2K'K_5K_2(\zeta)(1+\zeta)^{1/2}\Delta c}{DT_e \sin\bar{\alpha}_{\alpha,\beta}\left(\frac{\zeta V_\alpha}{L_\alpha m_\alpha} + \frac{V_\beta}{L_\beta m_\beta}\right)} \quad \text{(A2)}$$

An estimate of K_5 from first principles may be obtained if one utilises an expression for σ on the basis of corresponding states [21] connecting the solid-liquid interface energy with the latent heat of fusion:

$$\sigma_{\alpha,\beta-l} = 0.5\, L_{\alpha,\beta} \text{ (energy unit/atom)}$$

To express σ in erg/cm² and L in cal/mol, this equation must be modified in the following manner

$$\bar{\sigma}_{\alpha,\beta-l} = \frac{0.5K'L_{\alpha,\beta}}{N_L^{1/3} V_{\alpha,\beta}^{2/3}}$$

where

K' = conversion factor (4.186×10^7 erg/cal).

N_L = Avogadro's number (6.022×10^{23} atoms/mol). Equation A1 then becomes simply

$$K_5 = \frac{\sin\bar{\alpha}_{\alpha,\beta}}{4N_L^{1/3}} \cdot \frac{DT_e}{\Delta c K_2(\zeta)(1+\zeta)^{1/2}} \left[\frac{\zeta V_\alpha^{1/3}}{m_\alpha} + \frac{V_\beta^{1/3}}{m_\beta}\right] \cdot \quad \text{(A3)}$$

Equation A3 shows a simplification with respect to equation A1 in that both interface energy and latent heat of fusion disappear in favour of the molar volume. The term $\sin\bar{\alpha}_{\alpha,\beta}/4N_L^{1/3}$ is constant for $_{\alpha,\beta}\,\bar{\alpha} = 45°$ (2.1×10^{-9}).

References

1. F. R. MOLLARD and M. C. FLEMINGS, *Trans. AIME* **239** (1967) 1526.
2. P. R. SAHM, *J. Crystal. Growth* **6** (1969) 101.
3. K. A. JACKSON and J. D. HUNT, *Trans. AIME* **236** (1966) 1129.
4. J. D. LIVINGSTON, *J. Appl. Phys.* **41** (1970) 197.
5. B. C. ALLEN, *Trans. AIME* **227** (1963) 1175.
6. M. HANSEN and K. ANDERKO, "Constitution of Binary Alloys" (New York: McGraw Hill, 1958).
7. H. E. CLINE, *Trans. AIME* **242** (1968) 1613.
8. P. R. SAHM, *Schweizer Archiv* **36** (1970) 165.
9. B. LUX, Giesserei, *Techn. wiss. Beih.* **18** (1966) 219.
10. W. M. RUMBALL, *Metallurgia* (1968) 141.
11. D. D. DOUBLE, P. TRUELOVE, and A. HELLAWELL, *J. Crystal Growth* **2** (1969) 191.
12. M. J. SALKIND, F. D. GEORGE, F. D. LEMKEY, B. J. BAYLES and J. A. FORD, *Chem. Eng. Progr.* **62** (1969) 52.
13. A. MOORE and R. ELLIOT, *J. Inst. Metals* **96** (1968) 62.
14. A. MÜLLER and M. WILHELM, *J. Phys. and Chem. Solids* **26** (1965) 2029.
15. D. JAFFREY and G. A. CHADWICK, *Trans. AIME* **245** (1969) 2435.
16. P. R. SAHM, to be published: *J. Crystal Growth* (see also *Chemie-Ingenieur-Technik* **41** (1969) 1137).
17. H. R. KILLIAS, in print: *Chemie-Ingenieur-Technik* (1970).
18. H. P. UTECH and M. C. FLEMINGS, *J. Appl. Phys.* **37** (1966) 2021.

19. G. BUSCH and H. J. GÜNTHERODT, *Phys. Letters* **27A** (1968) 110 and to be published in *Proc. Solvay Congress, Brussels* (1969).
20. K. HIRANO, R. P. AGARWALA, B. L. AVERBACH, and M. COHEN, *J. Appl. Phys.* **33** (1962) 3049.
21. B. CHALMERS, "Physical Metallurgy" (New York, J. Wiley, 1959).

Received 16 July and accepted 12 August 1970.